Kinetics for Tautomerizations and Dissociations of Triglycine Radical Cations

ARTICLE *in* JOURNAL OF THE AMERICAN SOCIETY FOR MASS SPECTROMETRY · FEBRUARY 2009

Impact Factor: 2.95 · DOI: 10.1016/j.jasms.2009.01.014 · Source: PubMed

Kinetics for Tautomerizations and Dissociations of Triglycine Radical Cations

Chi-Kit Siu,[a] Junfang Zhao,[a] Julia Laskin,[b] Ivan K. Chu,[c] Alan C. Hopkinson,[a] and K. W. Michael Siu[a]

[a] Department of Chemistry and Centre for Research in Mass Spectrometry, York University, Toronto, Ontario, Canada
[b] Fundamental Sciences Division, Pacific Northwest National Laboratory, Richland, Washington, USA
[c] Department of Chemistry, University of Hong Kong, Hong Kong, China

Fragmentations of tautomers of the α-centered radical triglycine radical cation, $[GGG^{\bullet}]^{+}$, $[GG^{\bullet}G]^{+}$, and $[G^{\bullet}GG]^{+}$, are charge-driven, giving *b*-type ions; these are processes that are facilitated by a mobile proton, as in the fragmentation of protonated triglycine (Rodriquez, C. F. et al. J. Am. Chem. Soc. **2001**, *123*, 3006–3012). By contrast, radical centers are less mobile. Two mechanisms have been examined theoretically utilizing density functional theory and Rice-Ramsperger-Kassel-Marcus modeling: (1) a direct hydrogen-atom migration between two α-carbons, and (2) a two-step proton migration involving canonical $[GGG]^{\bullet+}$ as an intermediate. Predictions employing the latter mechanism are in good agreement with results of recent CID experiments (Chu, I. K. et al. J. Am. Chem. Soc. **2008,** *130*, 7862–7872). (J Am Soc Mass Spectrom 2009, 20, 996–1005) © 2009 American Society for Mass Spectrometry

Characterization and identification of a protein by means of mass spectrometry typically rely on fragmentation behaviors of its constituent fragment peptide ions in the gas phase [1–3]. Peptides are ionized by protonation via soft-ionization techniques: electrospray ionization [4] and matrix-assisted laser desorption/ionization [5]. Useful primary structural information of a peptide ion can then be obtained from fragmentations induced under low-energy conditions by slow-heating techniques [6], such as collision-induced dissociation (CID) [7, 8], infrared multiphoton dissociation (IRMPD) [9], and blackbody radiation [10]. The mechanisms by which protonated peptides dissociate have, therefore, generated much interest [11, 12]. Charge-driven amide bond cleavages are induced by the mobile proton, giving *b*- or *y*-type ions, which are, respectively, the N- or C-terminal fragments [1, 2]. By contrast, open-shell peptide radical cations produced in electron-capture [13–15] or electron-transfer dissociation experiments [16] give *c*- or *z*-type ions, by cleaving the N–C_{α} bond adjacent to the aminoketyl radical being formed [17–20]. The substantial fragmentation differences between protonated and radical cationic peptide provide useful complementary peptide sequencing information [21–23]. Ultraviolet (UV) photodissociation has also been employed for peptide fragmentation [24]. UV photodissociation of a peptide/protein chemically modified to incorporate an appropriate chromophore can generate a radical cation that undergoes site-specific, radical-driven dissociations, which are useful in protein identifications [25, 26]. Peptide radical cations have also been generated via low-energy CID of a ternary metal complex containing the peptide and auxiliary ligands [27–37]. These methodologies open new avenues whereby the fragmentation chemistries of peptide radical cations can be examined and exploited.

Dissociation at an amino-acid side chain is commonplace in the CID of peptide radical cations. These fragmentations are useful in providing differentiating signatures for isobaric residues present [14, 29, 38–40], e.g., between leucine and isoleucine [14, 29], and between aspartic acid and isoaspartic acid [38, 39]. For aromatic amino acid residues, cleavage of the C_{α}–C_{β} bond eliminates *p*-quinomethide from tyrosine and 3-methylene indolenine from tryptophan, yielding a glycyl radical with the unpaired electron located on the α-carbon [12, 27, 28, 30]. Such α-centered radicals have been identified in some anaerobic enzymes [41–43], including pyruvate formate-lyase [44, 45], anaerobic ribonucleotide reductase [46], benzylsuccinate synthase [47, 48], 4-hydroxyphenylacetate decarboxylase [49], and glycerol dehydratase [50]. A radical transfer from the thiyl group in the cysteine residue to a neighboring glycine residue by α-hydrogen-atom abstraction generates an α-centered radical [51, 52], which is stabilized by π-electron delocalization between the adjacent electron-withdrawing carbonyl group and the electron-donating amide nitrogen. This stabilization is known as the captodative effect [53]. The intrinsic stability of an amino-acid captodative radical has recently been verified by IRMPD spectroscopy on the histidine radical cation in the

Address reprint requests to Professor K.W.M. Siu, Department of Chemistry and Centre for Research in Mass Spectrometry, 4700 Keele St., Toronto, ON, Canada M3J 1P3. E-mail: kwmsiu@yorku.ca

1044-0305/09/$32.00
doi:10.1016/j.jasms.2009.01.014

Published online January 2, 2009
Received December 22, 2008
Revised January 20, 2009
Accepted January 21, 2009

gas phase [54]. Even the smallest, α-glycyl radical is stable and undergoes unimolecular dissociations with substantial threshold energies in the gas phase [55–57].

Radical migration in odd-electron ions produced by electron transfer and capture has been studied by several groups [58–63]. However, few detailed studies on the radical migration in radical cation $[M]^{\bullet+}$ have been performed [64–66]. A recent examination on the radical cations of the simplest tripeptide, $[GGG^{\bullet}]^+$, $[GG^{\bullet}G]^+$, and $[G^{\bullet}GG]^+$, showed that the barriers against radical migrations among these tautomers via transition structures having direct hydrogen transfer between two α-carbons are significantly higher than the barriers against proton migration in the analog protonated triglycine [65, 67]. Charge-driven amide bond cleavages are dominant in the CID of triglycine radical cations [65]. In this article, we report a two-step proton migration mechanism for tautomeric interconversions involving the canonical structure of triglycine radical cation as an intermediate. This two-step mechanism is then compared with the previously reported mechanism involving direct hydrogen-atom migration between α-carbons, utilizing density functional theory (DFT) and Rice-Ramsperger-Kassel-Marcus (RRKM) modeling.

Computational Details

The energy profiles for the interconversions between triglycine radical cations and their dissociations were taken from our previous studies [65]. All DFT calculations were performed on the Gaussian03 quantum chemical program [68] with the unrestricted (U) B3LYP functional [69, 70] and a Gaussian-type double-ζ 6-31++G(d,p) basis set [71, 72]. Minima and transition structures were characterized as such by means of harmonic frequency calculations. Anharmonicity scaling factors, 0.965 and 0.986, were applied to frequency and zero-point energy calculations, respectively [73]. Atomic charges were calculated using the natural population analysis [74].

The microcanonical rate constant $k_i(E)$ of each unimolecular reaction i was calculated using the Rice-Ramsperger-Kassel-Marcus (RRKM) equation [75, 76]. $k_i(E)$ is a function of the internal energy E of the reactant, relative to that of the structure at the global minimum on the potential energy surface (PES)

$$k_i(E) = \frac{\sigma W_i^{\ddagger}(E_i - E_{0i})}{h\rho_i(E_i)}$$

where $E_i = E - \Delta H_{0i}$ is the available vibrational energy and ΔH_{0i} is the i^{th} reactant's enthalpy of formation at 0 K, $\rho_i(E_i)$ is the density of vibrational states of the reactant, $W_i^{\ddagger}(E_i - E_{0i})$ is the sum of the vibrational states of the transition state, E_{0i} is the corresponding critical energy for reaction, h is Planck's constant, and σ is the reaction path degeneracy, which is one in all the reactions examined herein. The vibrational states were directly counted using the Beyer-Swinehart algorithm [77].

Results and Discussion

RRKM Modeling and Kinetic Approximations

On the PES of $[GGG + H]^+$, rotamers are close in energy and separated via relatively low interconversion barriers (<17 kcal mol^{-1}) involving bond rotations and proton transfers [67]. As the mobile proton migrates to the nitrogen atom of an amide bond, peptide-bond cleavage can occur via a transition structure with higher energy (32 kcal mol^{-1}) resulting in the b_2^+ product ion [67]. The PES for the interconversions of triglycine radical cations has been examined by DFT calculations [65]; notably, the barriers against interconversions are typically larger than those against bond cleavages, contrary to the observations in protonated triglycine where the barriers against tautomerisms are much lower than those against dissociations [67]. A simplified version of the PES for $[GGG^{\bullet}]^+$ (the radical being located on the α-carbon at the C-terminus) is shown in Figure 1a (see reference 65 and Figure S1 in the Supporting Information for the structures, which can be found in the electronic version of this article). The lowest-energy structure is $[\mathbf{GGG^{\bullet}}]^+$**-1**, where the proton is attached to the amide oxygen of the N-terminal peptide bond and the radical is centered at the α-carbon in the C-terminal residue. Proton migration together with rotation about the C–C bond in the central residue forms $[\mathbf{GGG^{\bullet}}]^+$**-7** at a shallow minimum, followed by rotation about the C=O bond to form $[\mathbf{GGG^{\bullet}}]^+$**-3**. Further rotation about the C–C bond of the C-terminal residue results in $[\mathbf{GGG^{\bullet}}]^+$**-6**, the precursor of the $[\mathbf{b_3 - H}]^{\bullet+}$**-2** fragment ion produced by the loss of a water molecule. The barriers against interconversions among the $[GGG^{\bullet}]^+$ isomers are between 24 and 27 kcal mol^{-1}, which is slightly lower than the barrier against water loss at 32.6 kcal mol^{-1}. A competitive dissociation channel is the one that gives the b_2^+ ion, by losing a neutral $[Gly - H]^{\bullet}$ directly from $[\mathbf{GGG^{\bullet}}]^+$**-1**, against a barrier of 36.0 kcal mol^{-1}.

The competition between the two dissociation channels on the PES as shown in Figure 1a is examined by kinetic analyses employing the RRKM theory to model the unimolecular rate constants of each elementary reaction (k_i's). The full kinetics of this quadruple-well-two-exit (4 well-2 exit) PES model is thus represented by a set of equations (eq1) for the rates of change ($\dot{I}_i$) of the relative abundance of ion i (I_i) with respect to the reaction time t.

$$\begin{aligned}
\dot{I}_1 &= -(k_{A1} + k_{A8})I_1 + k_{A2}I_7 \\
\dot{I}_7 &= k_{A1}I_1 - (k_{A2} + k_{A3})I_7 + k_{A4}I_3 \\
\dot{I}_3 &= k_{A3}I_7 - (k_{A4} + k_{A5})I_3 + k_{A6}I_6 \\
\dot{I}_6 &= k_{A5}I_3 - (k_{A6} + k_{A7})I_6 \\
\dot{I}_{P1} &= k_{A7}I_6 \\
\dot{I}_{P2} &= k_{A8}I_1
\end{aligned} \quad (1)$$

Applying RRKM modeling, the microcanonical rate constants, $k_{A1} - k_{A8}$, are evaluated as a function of the

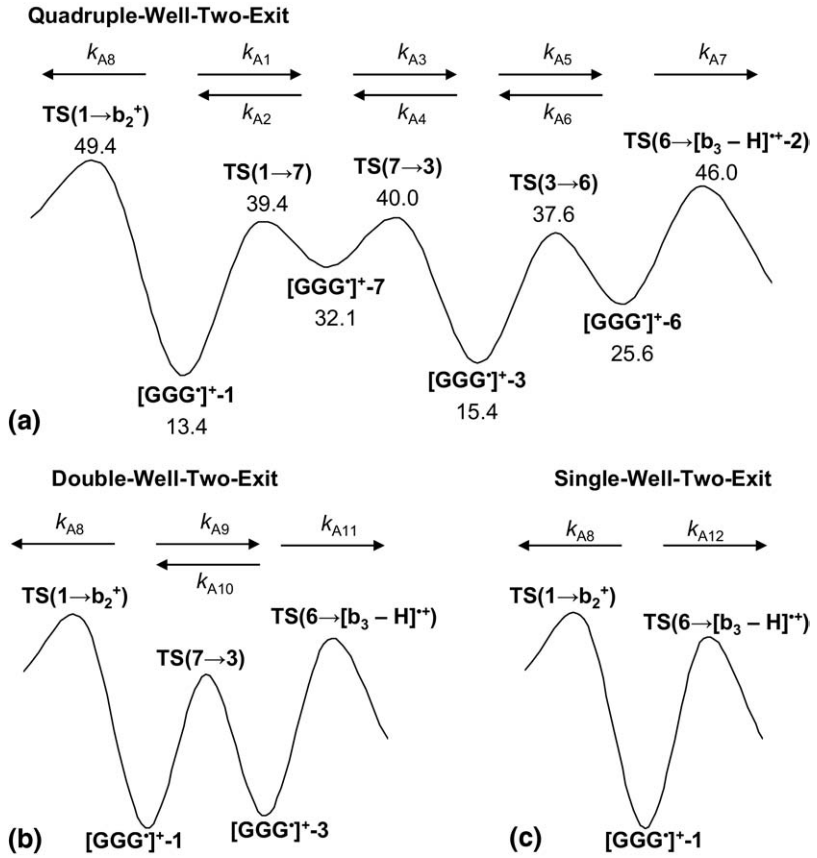

Figure 1. Potential energy surface (PES) for the isomerizations and dissociations of $[GGG^\bullet]^+$. (**a**) Full PES including bond rotation and proton-transfer reactions as reported in reference 65; (**b**) PES with only isomers $[\mathbf{GGG^\bullet}]^+$-**1** and **3**; (**c**) PES with only isomer 1 $[\mathbf{GGG^\bullet}]^+$-**1**. Enthalpies ΔH°_0 (in kcal mol^{-1}) are relative to the lowest-energy isomer of $[G^\bullet GG]^+$ and evaluated at the unrestricted B3LYP/6-31++G(d,p) level.

internal energy E (relative to the lowest energy tautomer $[G^\bullet GG]^+$) and shown in Figure 2. $[\mathbf{GGG^\bullet}]^+$-**7** is located in a shallow minimum on the PES; this ion undergoes fast isomerization to either $[\mathbf{GGG^\bullet}]^+$-**1** or $[\mathbf{GGG^\bullet}]^+$-**3**, and k_{A2} and k_{A3} have the largest values of all rate constants under all internal energies. Similarly, $[\mathbf{GGG^\bullet}]^+$-**6** is quickly isomerized to $[\mathbf{GGG^\bullet}]^+$-**3**, as also indicated by the large values of k_{A6} (Figure 2a).

Three approaches have been used to solve the set of differential equations (eq 1) by applying: (1) numerical integration; (2) steady-state approximation with $[\mathbf{GGG^\bullet}]^+$-**7**, and $[\mathbf{GGG^\bullet}]^+$-**6** treated as intermediates (SSA1), i.e., $\dot{I}_7 = \dot{I}_6 = 0$; and (3) steady-state approximation with all minima, except $[\mathbf{GGG^\bullet}]^+$-**1**, treated as intermediates (SSA2), i.e., $\dot{I}_7 = \dot{I}_3 = \dot{I}_6 = 0$. For SSA1, Equations 1 are reduced to eq S1-1 (see Supporting Information) and can be solved analytically resulting in solutions of I_i with respect to the reaction time t (eq S1-2). The rate equations can be further reduced by SSA2, resulting in simple first-order kinetics eq S2-1 and the solutions shown in eq S2-2.

Figure 3 shows the relative abundance of ions I_i equations (eq 1) as a function of internal energy E obtained from all integration approaches at a reaction time $t = 30$ ms, corresponding to the activation time for the CID experiments described in reference 65. The initial reactant is assumed to be exclusively the $[\mathbf{GGG^\bullet}]^+$-**1** ion on the PES as shown in Figure 1, i.e., $I_1 = 1 \; and \; I_7 = I_3 = I_6 = 0 \; at \; t = 0$. As E increases, isomerization occurs and equilibrium is established between $[\mathbf{GGG^\bullet}]^+$-**1** and $[\mathbf{GGG^\bullet}]^+$-**3** (Figure 3a). As expected from Figure 1, the abundances of structures at the shallow minima $[\mathbf{GGG^\bullet}]^+$-**7** and $[\mathbf{GGG^\bullet}]^+$-**6** are negligibly small and are ≤0.1% (data not shown). No dissociation products are evident before $E = 50$ kcal mol^{-1}; thereafter $[b_3 - H]^{\bullet+}$ (Figure 3b) and b_2^+ (Figure 3c) emerge, with the former product ion peaking in abundance at ~60 kcal mol^{-1}. Employing steady-state approximations perturbs the kinetics minimally and provides analytical solutions to the first-order differential equations.

In fragmentations of protonated peptides, energies of the transition structures associated with peptide bond cleavages are higher than those for bond rotations and proton transfers [67]. The transition structure leading to bond cleavages thus constitutes the critical step, permitting simplification to, and approximation as, first-order kinetics regardless of the number of steps involved.

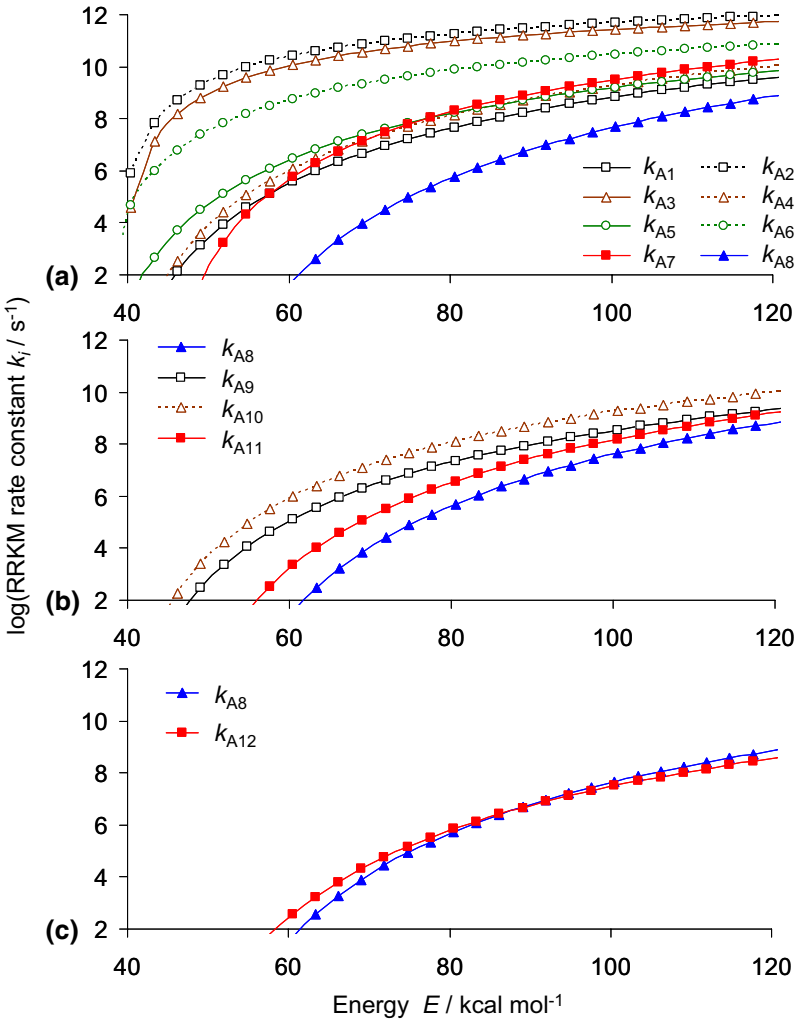

Figure 2. RRKM rate constants, log k_i/s^{-1}, versus internal energies E/kcal mol^{-1} for $[GGG^{\bullet}]^+$: (**a**) k_{A1}–k_{A8}, (**b**) k_{A8}–k_{A11}, and (**c**) k_{A8} and k_{A12}.

Here we examine the effects of kinetics using $[GGG^{\bullet}]^+$ as a prototypical example for peptide radical cations. Based on the results shown in Figure 2, the quadruple-well-two-exit (4 well-2 exit) PES (Figure 1a) of $[GGG^{\bullet}]^+$ can readily be simplified to a double-well-two-exit (2 well-2 exit) PES (Figure 1b), in which the shallow minima **[GGG•]$^+$-7** and **[GGG•]$^+$-6** and the associated transition structures having lower energies [**TS(1→7)** and **TS(3→6)**] are ignored. The resulting rate equations and their solutions (eqs S3-1 and S3-2, respectively) are similar to those for SSA1, in which the seven rate constants k_{A1}–k_{A7} are approximated by the three rate constants k_{A9}–k_{A11} (Figure 2b). This simplification has virtually no effects on the relative abundances at low E (Figure 3). For $E > 80$ kcal mol^{-1}, small differences are observed between the relative abundances of product ions predicted by the full PES and those by the simplified models. These differences increase with increasing E, resulting in overestimating the abundance of $[b_3 - H]^{\bullet+}$ (Figure 3b), whose formation involves more intermediate steps than that of b_2^+ (Figure 3c). The latter involves only a single step and the 2 well-2 exit model results in underestimating the abundance of b_2^+. Further approximation to a single-well-two-exit (1 well-2 exit) system, in which only one rate constant k_{A12} is used instead of the seven rate constants k_{A1}–k_{A7} (Figure 1c and Figure 2c, and eqs S4-1 and S4-2 in the Supporting Information), affords further simplification, but also introduces additional albeit small errors. Importantly, using the transition structure of the highest energy as the critical step instead of the full reaction path introduces only small errors to the relative abundances of the product ions, and this approximation greatly simplifies the calculations.

Direct Hydrogen-Atom Migration Between Two α-Carbons

Compared with the mobile proton in a protonated triglycine, the radical center on the α-carbon of a triglycine radical cation is relatively immobile; this has

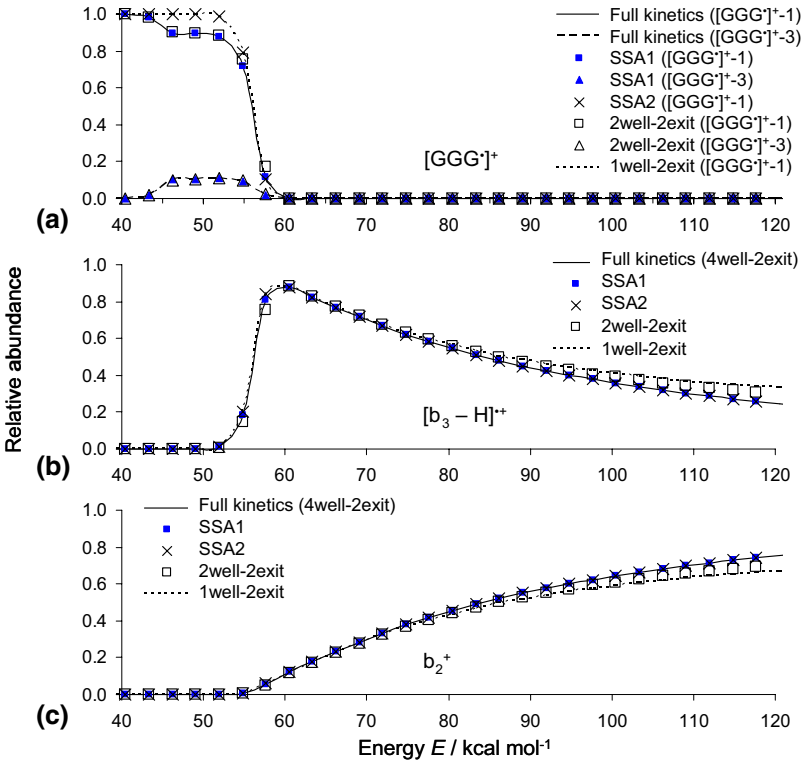

Figure 3. Relative abundances of (**a**) $[\mathbf{GGG^{\bullet}}]^+$-**1** and $[\mathbf{GGG^{\bullet}}]^+$-**3**, (**b**) **P1**$[\mathbf{b_3}-\mathbf{H}]^{\bullet+}$-**2**, and (**c**) **P2** b_2^+ calculated based on the energy profiles including full kinetics, steady-state approximations 1 and 2 (SSA1 and SSA2) (Figure 1a), double-well-two-exit (2 well-2 exit) (Figure 1b), and single-well-two-exit (1 well-2 exit) (Figure 1c). Reaction time t = 30 ms.

recently been demonstrated by the very different CID spectra of $[GGG^{\bullet}]^+$, $[GG^{\bullet}G]^+$, and $[G^{\bullet}GG]^+$ [65]. Interconversions among these isomers are possible but direct hydrogen-atom migrations between the α-carbons were found to have higher barriers than dissociations in general. Figure 4a summarizes the interconversion reactions and shows the structures of the lowest-energy isomers and critical transition states proposed in reference 65 ($[\mathbf{GGG^{\bullet}}]^+$-**1**, $[\mathbf{GG^{\bullet}G}]^+$-**1**, and $[\mathbf{G^{\bullet}GG}]^+$-**1** used previously are now also denoted as **A**, **B**, and **C**, respectively, for simplicity). The DFT-computed charges of the migrating hydrogen were 0.23–0.25 [natural population analyses at UB3LYP/6-31++G(d,p)], which characterized these transfers as hydrogen-atom migrations. The dissociations of the triglycine radical cations were charge-driven [65]: $[G^{\bullet}GG]^+$ gave only a single product, $[b_2 - H]^{\bullet+}$; $[GG^{\bullet}G]^+$ gave two products, $[b_2 - H]^{\bullet+}$, and $[b_3 - H]^{\bullet+}$, the latter by the loss of water; and $[GGG^{\bullet}]^+$ gave $[b_2 - H]^{\bullet+}$, $[b_3 - H]^{\bullet+}$, and b_2^+ (the last with $[Gly - H]^{\bullet}$ as the neutral product). Notably, formation of $[b_2 - H]^{\bullet+}$ required first isomerization of **A** to **B** or **C**. Table 1 summarizes the energetics of the isomerization and dissociation reactions [65]. The barriers against interconversions via direct hydrogen-atom migrations between two α-carbons (reactions of k_{B7}–k_{B12}) are in general higher than those against dissociations (reactions of k_{B1}–k_{B6}). Many of these reactions involve consecutive isomerizations via transition structures with lower energies compared with the critical tautomerization or dissociation steps. As discussed in the previous section, the potential-energy surfaces of these reactions can be much simplified by considering only the critical steps.

Scheme 1 shows the results of such simplification as a triple-well-six-exit PES. The rate equations and the rate constants as a result of RRKM modeling are shown in eq S5 in the Supporting Information. Compared with the rates of isomerization reactions involving bond rotations and proton transfers (Figure 2), the tautomerization reactions are a few orders of magnitude slower (Figure S3). To examine the competition between tautomerizations and dissociations, eq S5 are thus solved numerically at each internal energy E with a reaction time t = 30 ms; the results are shown in Figure 5: initial conditions at t = 0, (a)I_A = 1 *and* I_B = I_C = 0, (b) I_B = 1 *and* I_A = I_C = 0, and (c) I_C = 1 *and* I_A = I_B = 0. For isomerically pure **A** (Figure 5a), the dissociation barrier leading to $[b_3 - H]^{\bullet+}$ (specifically $[b_3 - H]^{\bullet+}$-**2**) and water (k_{B1}) is 46.0 kcal mol^{-1}, only 3.4 kcal mol^{-1} lower than that against the formation of b_2^+ and $[Gly - H]^{\bullet}$ (k_{B2}) (see Table 1). Thus the two channels are competitive under CID conditions; the former channel has a negative activation entropy ($\Delta S^{\ddagger}_{298}$ = −0.7 cal mol^{-1} K^{-1}) whereas the latter has a positive value ($\Delta S^{\ddagger}_{298}$ = 5.4 cal mol^{-1} K^{-1}), resulting in $[b_3 - H]^{\bullet+}$ being less abundant than b_2^+ at larger internal energies and, therefore, becomes more abundant at large E. Figure 5a

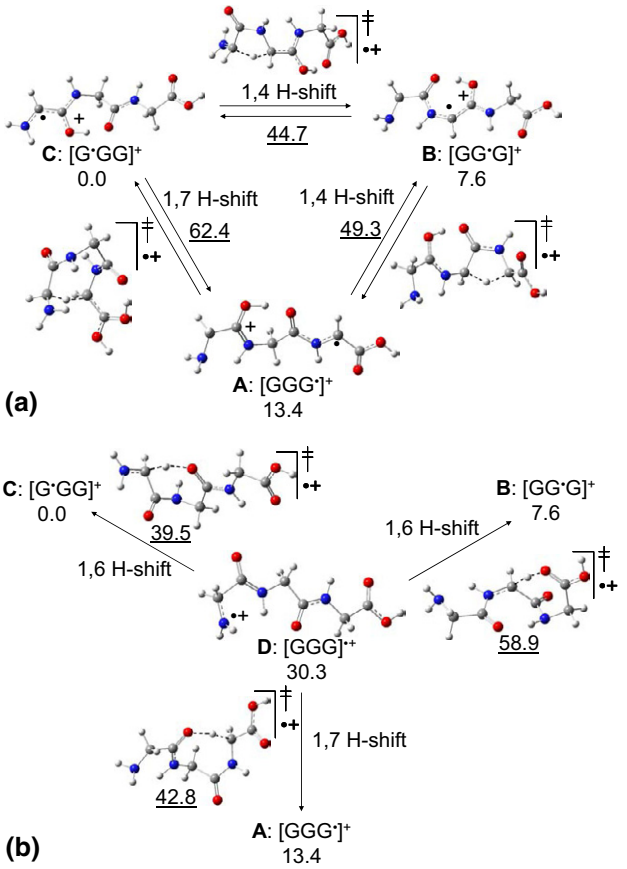

Figure 4. Optimized geometries of the lowest-energy tautomers and transition structures for interconversion between $[GGG^{\bullet}]^+$ (**A**), $[GG^{\bullet}G]^+$ (**B**), and $[G^{\bullet}GG]^+$ (**C**): (**a**) direct hydrogen-atom migration; (**b**) two-step proton migration via canonical $[GGG]^{\bullet+}$ as an intermediate. Enthalpies ΔH°_0 (in kcal mol^{-1}) are relative to the lowest-energy isomer of $[G^{\bullet}GG]^+$ and evaluated at UB3LYP/6-31++G(d,p) level.

shows this crossover point at $E \approx 85$ kcal mol^{-1}. Similarly, isomerically pure **B** (Figure 5b) can dissociate to give $[b_3 - H]^{\bullet+}$-**1** (k_{B3}) or $[b_2 - H]^{\bullet+}$-**2** (k_{B4}). Interestingly, **B** can convert to **C** which fragments to $[b_2 - H]^{\bullet+}$-**1**, a lower-energy isomer of $[b_2 - H]^{\bullet+}$-**2**. In fact, the barrier against interconversion of **B** to **C** is lower than that against the two fragmentation reactions of **B**; this means that at low E, the product $[\mathbf{b_2}-\mathbf{H}]^{\bullet+}$-**1** from **C** is preferentially formed over its isomer $[b_2 - H]^{\bullet+}$-**2** from **B**. At $E > 95$ kcal mol^{-1}, the dominant product ion becomes $[b_2 - H]^{\bullet+}$-**2**; this dissociation (k_{B4}) has a positive activation entropy ($\Delta S^{\ddagger}_{298}$) of 2.9 cal mol^{-1} K^{-1}. By contrast, the similar dissociation from **C** (k_{B6}) has a negative $\Delta S^{\ddagger}_{298} = -1.7$ cal mol^{-1} K^{-1}, as did tautomerization from **B** to **C** (k_{B9}, $\Delta S^{\ddagger}_{298} = -0.1$ cal mol^{-1} K^{-1}) and that from **C** to **B** (k_{B10}, $\Delta S^{\ddagger}_{298} = -9.5$ cal mol^{-1} K^{-1}). Formation of the b_2^+ ion from **B** requires a tautomerization from **B** to **A**, which is both thermodynamically and kinetically unfavorable. Consequently, the relative abundance of b_2^+ formed from **B** is low and <2.5% for E up to 200 kcal mol^{-1} (data not shown).

Figure 5c shows that isomerically pure **C** dissociates solely to give $[b_2 - H]^{\bullet+}$-**1**. The loss of water from **C** to give $[b_3 - H]^{\bullet+}$-**3** (k_{B5}) is not competitive and occurs only at high E, contributing only around 1% of the total ion abundance at $E = 100$ kcal mol^{-1} and only 10% at $E = 200$ kcal mol^{-1} (the latter data not shown). Tautomerization from **C** to **B** or **A** is also negligible; the total abundance of the product ions fragmented from tautomeric isomers **B** and **C** is <0.1% at $E = 100$ kcal mol^{-1} and 3% at $E = 200$ kcal mol^{-1} (the latter not shown).

In general, results of the above kinetic examinations are consistent with those of the CID experiments [65]: **C** dissociates to give $[b_2 - H]^{\bullet+}$; **B** to $[b_2 - H]^{\bullet+}$ and $[b_3 - H]^{\bullet+}$ ions; and **A** to $[b_3 - H]^{\bullet+}$ and b_2^+. However, the abundant $[b_2 - H]^{\bullet+}$ as observed in the dissociation of **A** is not compatible with the RRKM kinetics determined above, which predicts the relative abundance of $[b_2 - H]^{\bullet+}$ to be <1.5% for all E up to 200 kcal mol^{-1}. Additionally, the calculated low abundance of $[b_2 - H]^{\bullet+}$ from the dissociation of **A** is independent of the reaction time t chosen for integration of the rate equations. This is evidenced by the relative abundances of the product ions obtained by solving eq S5 with reaction time t ranging from 0.1 μs to 100 ms (Figure S4 in the Supporting Information). As expected, increasing the reaction time shifts the dissociation thresholds to lower E, while the total relative abundance of the $[b_2 - H]^{\bullet+}$ ion remains <2%. This discrepancy is resolved via a more sophisticated PES involving canonical $[GGG]^{\bullet+}$ as an intermediate during tautomerization (vide infra).

Two-Step Proton Migration Involving Canonical $[GGG]^{\bullet+}$ During Tautomerization

The optimized canonical $[GGG]^{\bullet+}$ structure is **D**, shown in Figure 4b. Notably, the migrating hydrogens in the transition structures carry positive charges 0.35–0.43, which are considerably larger than those for direct hydrogen-atom migration between two α-carbons (0.23–0.25) described in the previous section. For this reason, the isomerization reactions involving **D** are more appropriately described as proton-transfer reactions. Isomer **D** is 30.3 kcal mol^{-1} higher in enthalpy than the most-stable isomer **C**. Nevertheless, isomer **D** catalyzes some of the interconversion reactions: interconversion between **A** and **C** is significantly facilitated by reducing the original barrier of 62.4 kcal mol^{-1} to 42.8 kcal mol^{-1} for the current two-step proton migration involving isomer **D** as an intermediate.

Reactions denoted by the rate constants k_{B13}–k_{B18} in Scheme 1 are interconversions among **A**, **B**, and **C**, involving **D** as an intermediate. The modified kinetics is summarized in eq S6 in the Supporting Information. The relative abundances of the ions are obtained by solving eq S6 numerically with a reaction time $t = 30$ ms; the results are shown in Figure 5d–f. For isomerically pure **B** and **C**, the presence of the canonical isomer

Table 1. Relative energies at 0 K (ΔH°_0/kcal mol^{-1}) of tautomers of the triglycine radical cation, their dissociation products, and activation barriers at 0 K ($\Delta H^{\ddagger}_0$/kcal mol^{-1}) and entropies at 298 K ($\Delta S^{\ddagger}298$/cal mol^{-1} K^{-1}). All energies are relative to the lowest-energy tautomer [G*GG]$^+$ (C) and performed at the UB3LYP/6-31++G(d,p) level

Relative energies of tautomers		Relative energies of products	
	ΔH°_0		ΔH°_0
[GGG]$^{\cdot+}$ (A)	13.4	[b_3 − H]$^{\cdot+}$ −2 + H_2O (P1)	37.1
[GGG]$^{\cdot+}$ (B)	7.6	b_2^+ + [Gly − H]$^{\cdot}$ (P2)	40.6
[GGG]$^{\cdot+}$ (C)	0.0	[b_3 − H]$^{\cdot+}$ −1 + H_2O (P3)	28.8
[GGG]$^{\cdot+}$ (D)	30.3	[b_2 − H]$^{\cdot+}$ −2 + Gly (P4)	50.8
		[b_3 − H]$^{\cdot+}$ −3 + H_2O (P5)	29.3
		[b_2 − H]$^{\cdot+}$ −1 + Gly (P6)	33.0

Dissociation barriers				Interconversion barriers							
	Rate constant	$\Delta H^{\ddagger}_0$	$\Delta S^{\ddagger}_{298}$		Rate constant	$\Delta H^{\ddagger}_0$	$\Delta S^{\ddagger}_{298}$		Rate constant	$\Delta H^{\ddagger}_0$	$\Delta S^{\ddagger}_{298}$
A → P1	k_{B1}	46.0	−0.7	A → B	k_{B7}	49.3	−2.3	A → D	k_{B13}	42.8	−3.1
A → P2	k_{B2}	49.4	5.4	A ← B	k_{B8}		−1.6	A ← D	k_{B14}		−10.6
B → P3	k_{B3}	48.5	−0.9	B → C	k_{B9}	44.7	−0.1	B → D	k_{B15}	58.9	−3.6
B → P4	k_{B4}	43.3	2.9	B ← C	k_{B10}		−9.5	B ← D	k_{B16}		−9.7
C → P5	k_{B5}	44.3	7.7	C → A	k_{B11}	62.4	−8.5	C → D	k_{B17}	39.5	−3.1
C → P6	k_{B6}	29.6	−1.7	C ← A	k_{B12}		−8.5	C ← D	k_{B18}		−9.6

D has negligible effects: Interconversion between **B** and **D** is blocked by a high-energy barrier of 58.9 kcal mol^{-1}. The interconversion barrier between **C** and **D** is moderate, only 39.5 kcal mol^{-1}, but is still significantly higher than the energy required for dissociating **C** to give [b_2 – H]$^{\bullet+}$-**1** (33.0 kcal mol^{-1}). By contrast, the interconversion from **A** to **C** is significantly enhanced via isomer **D** as an intermediate, resulting in significant abundance of [b_2 − H]$^{\bullet+}$-1 in Figure 5d versus <1.5% in Figure 5a. Thus the PES composed by all reactions k_{B1}–k_{B18} provides an accurate description of the CID experiments. We will refrain from over-interpreting by attempting to draw quantitative correlations between experimental and RRKM-derived ion abundances.

Conclusion

Tautomerizations and dissociations of radical cations of tripeptides—[GGG$^{\bullet}$]$^+$, [GG$^{\bullet}$G]$^+$, and [G$^{\bullet}$GG]$^+$—have been examined theoretically employing DFT calculations and RRKM modeling. The PES of each of these tautomers comprises many low-lying rotamers that

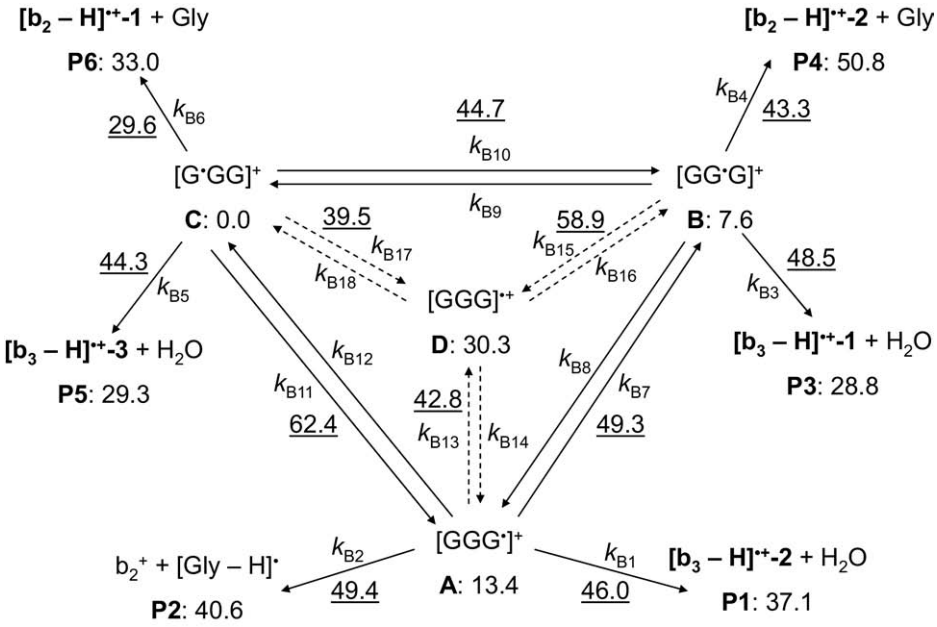

Scheme 1. Tautomerizations and dissociations of the triglycine radical cation. Relative enthalpies ΔH°_0 (in kcal mol^{-1}) are evaluated at the UB3LYP/6-31++G(d,p) level. The underlined values are critical energy barriers. The reactions for the two-step proton migration mechanism via canonical [GGG]$^{\bullet+}$ are placed within the inverted "triangle" and signified by arrows with dashed lines.

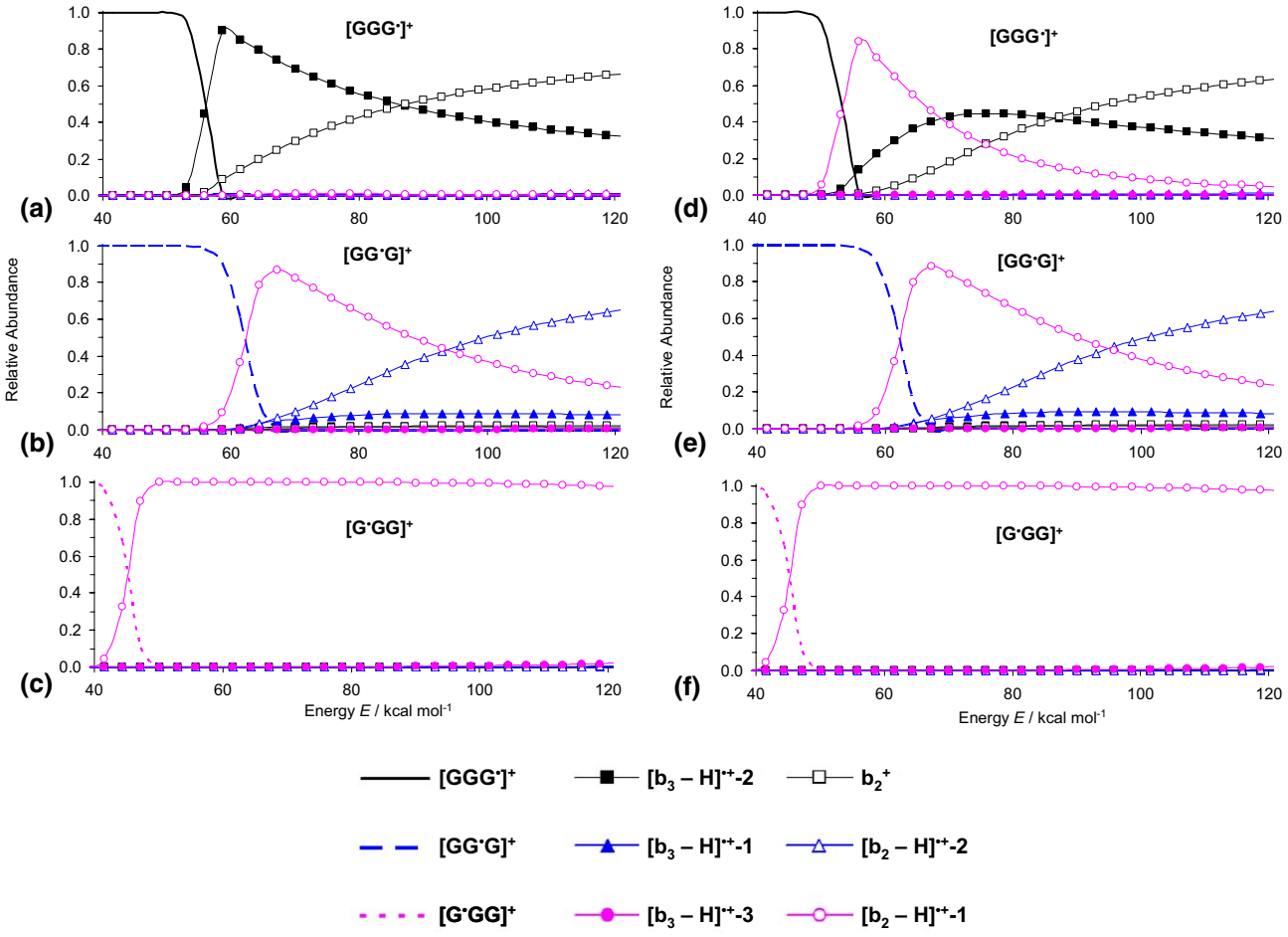

Figure 5. Relative abundances of ions with initial conditions (**a**) $I_A = 1$ *and* $I_B = I_C = 0$, (**b**) $I_B = 1$ *and* $I_A = I_C = 0$, and (**c**) $I_C = 1$ *and* $I_A = I_B = 0$ for direct hydrogen-atom migration; and (**d**) $I_A = 1$ *and* $I_B = I_C = 0$, (**e**) $I_B = 1$ *and* $I_A = I_C = 0$, and (**f**) $I_C = 1$ *and* $I_A = I_B = 0$ for two-step proton-migration via canonical $[GGG]^{\bullet+}$. Reaction time $t = 30$ ms.

are interconvertible via transition structures involving bond rotations and hydrogen transfers. In spite of these barriers being higher than those of analogous isomerizations in protonated triglycine [67], they are still lower than those against dissociations and contribute little to the overall kinetics, as verified by RRKM calculations. Only the critical step with highest barrier is important. By contrast, interconversions between $[GGG^{\bullet}]^+$, $[GG^{\bullet}G]^+$, and $[G^{\bullet}GG]^+$ involving radical migration require transition structures with energies comparable to the dissociation barriers. Two mechanisms for such interconversions have been developed and discussed: (1) direct hydrogen-atom migration between two α-carbons, and (2) two-step proton migration involving canonical $[GGG]^{\bullet+}$ as an intermediate. Interconversion between $[GGG^{\bullet}]^+$ and $[G^{\bullet}GG]^+$ is enhanced in the latter mechanism that has a critical barrier of 42.8 kcal mol^{-1} versus 62.4 kcal mol^{-1} in the former. The consequence of this lower barrier is significant, as predicted $[b_2 - H]^{\bullet+}$ abundance is now much higher for $[GGG^{\bullet}]^+$, and in agreement with CID experiments [65].

Acknowledgments

This work was made possible by funding from the Natural Sciences and Engineering Research Council (NSERC) of Canada and by the facilities of the Shared Hierarchical Academic Research Computing Network (SHARCNET: www.sharcnet.ca). The authors thank the Department of Mathematics and Statistics, York University, for granting access to the MATHSTAT time sharing server. Part of this work was conducted in the Environmental Molecular Science Laboratory, located at the Pacific Northwest National Laboratory, and operated for the U.S. Department of Energy (DOE) by Battelle, during CKS's visit with JL. JL acknowledges the support from the Chemical Sciences Division, Office of Basic Energy Sciences of the U.S. DOE.

Appendix A. Supplementary Material

Supplementary material associated with this article may be found in the online version at doi:10.1016/j.jasms.2009.01.014.

References

1. Roepstorff, P.; Fohlman, J. Proposal for a Common Nomenclature for Sequence Ions in Mass-Spectra of Peptides. *Biomed. Mass Spectrom.* **1984,** *11,* 601–601.
2. Biemann, K.; Martin, S. A. Mass-Spectrometric Determination of the Amino-Acid-Sequence of Peptides and Proteins. *Mass Spectrom. Rev.* **1987,** *6,* 1–75.
3. Aebersold, R.; Goodlett, D. R. Mass Spectrometry in Proteomics. *Chem. Rev.* **2001,** *101,* 269–295.
4. Fenn, J. B.; Mann, M.; Meng, C. K.; Wong, S. F.; Whitehouse, C. M. Electrospray Ionization for Mass-Spectrometry of Large Biomolecules. *Science* **1989,** *246,* 64–71.
5. Karas, M.; Hillenkamp, F. Laser Desorption Ionization of Proteins with Molecular Masses Exceeding 10,000 Daltons. *Anal. Chem.* **1988,** *60,* 2299–2301.
6. McLuckey, S. A.; Goeringer, D. E. Slow Heating Methods in Tandem Mass Spectrometry. *J. Mass Spectrom.* **1997,** *32,* 461–474.
7. Smith, R. D.; Loo, J. A.; Barinaga, C. J.; Edmonds, C. G.; Udseth, H. R. Collisional Activation and Collision-Activated Dissociation of Large Multiply Charged Polypeptides and Proteins Produced by Electrospray Ionization. *J. Am. Soc. Mass Spectrom.* **1990,** *1,* 53–65.
8. Laskin, J.; Futrell, J. H. Collisional Activation of Peptide Ions in FT-ICR Mass Spectrometry. *Mass Spectrom. Rev.* **2003,** *22,* 158–181.
9. Little, D. P.; Speir, J. P.; Senko, M. W.; O'Connor, P. B.; McLafferty, F. W. Infrared Multiphoton Dissociation of Large Multiply-Charged Ions for Biomolecule Sequencing. *Anal. Chem.* **1994,** *66,* 2809–2815.
10. Price, W. D.; Schnier, P. D.; Williams, E. R. Tandem Mass Spectrometry of Large Biomolecule Ions by Blackbody Infrared Radiative Dissociation. *Anal. Chem.* **1996,** *68,* 859–866.
11. Paizs, B.; Suhai, S. Fragmentation Pathways of Protonated Peptides. *Mass Spectrom. Rev.* **2005,** *24,* 508–548.
12. Wysocki, V. H.; Cheng, G.; Zhang, Q.; Hermann, K. A.; Beardsley, R. L.; Hilderbrand, A. E. Peptide Fragmentation Overview. In *Principles of Mass Spectrometry Applied to Biomolecules*, Laskin, J.; Lifshitz, C., Eds.; Wiley-Interscience: Hoboken, NJ, 2006; p. 279.
13. Zubarev, R. A.; Kelleher, N. L.; McLafferty, F. W. Electron Capture Dissociation of Multiply Charged Protein Cations. A Nonergodic Process. *J. Am. Chem. Soc.* **1998,** *120,* 3265–3266.
14. Zubarev, R. A. Reactions of Polypeptide Ions with Electrons in the Gas Phase. *Mass Spectrom. Rev.* **2003,** *22,* 57–77.
15. Cooper, H. J.; Hakansson, K.; Marshall, A. G. The Role of Electron Capture Dissociation in Biomolecular Analysis. *Mass Spectrom. Rev.* **2005,** *24,* 201–222.
16. Syka, J. E. P.; Coon, J. J.; Schroeder, M. J.; Shabanowitz, J.; Hunt, D. F. Peptide and Protein Sequence Analysis by Electron Transfer Dissociation Mass Spectrometry. *Proc. Natl. Acad. Sci. U.S.A.* **2004,** *101,* 9528–9533.
17. Tureček, F. N–C_α Bond Dissociation Energies and Kinetics in Amide and Peptide Radicals. Is the Dissociation a Nonergodic Process? *J. Am. Chem. Soc.* **2003,** *125,* 5954–5963.
18. Syrstad, E. A.; Tureček, F. Toward a General Mechanism of Electron Capture Dissociation. *J. Am. Soc. Mass Spectrom.* **2005,** *16,* 208–224.
19. Sobczyk, M.; Anusiewicz, W.; Berdys-Kochanska, J.; Sawicka, A.; Skurski, P.; Simons, J. Coulomb-Assisted Dissociative Electron Attachment: Application to a Model Peptide. *J. Phys. Chem. A.* **2005,** *109,* 250–258.
20. Skurski, P.; Sobczyk, M.; Jakowski, J.; Simons, J. Possible Mechanisms for Protecting N–C_α Bonds in Helical Peptides from Electron-Capture (or Transfer) Dissociation. *Int. J. Mass Spectrom.* **2007,** *265,* 197–212.
21. Zubarev, R. A.; Horn, D. M.; Fridriksson, E. K.; Kelleher, N. L.; Kruger, N. A.; Lewis, M. A.; Carpenter, B. K.; McLafferty, F. W. Electron Capture Dissociation for Structural Characterization of Multiply Charged Protein Cations. *Anal. Chem.* **2000,** *72,* 563–573.
22. Hopkinson, A. C.; Siu, K. W. M. Peptide Radical Cations. In *Principles of Mass Spectrometry Applied to Biomolecules*, Laskin, J.; Lifshitz, C., Eds.; John Wiley and Sons, Inc.: Hoboken, 2006; p. 301.
23. Barlow, C. K.; O'Hair, R. A. J. Gas-Phase Peptide Fragmentation: How Understanding the Fundamentals Provides a Springboard to Developing New Chemistry and Novel Proteomic Tools. *J. Mass Spectrom.* **2008,** *43,* 1301–1319.
24. Gabryelski, W.; Li, L. Photo-Induced Dissociation of Electrospray Generated Ions in an Ion Trap. *Rev. Sci. Instrum.* **1999,** *70,* 4192–4199.
25. Ly, T.; Julian, R. R. Residue-Specific Radical-Directed Dissociation of Whole Proteins in the Gas Phase. *J. Am. Chem. Soc.* **2008,** *130,* 351–358.
26. Diedrich, J. K.; Julian, R. R. Site-Specific Radical Directed Dissociation of Peptides at Phosphorylated Residues. *J. Am. Chem. Soc.* **2008,** *130,* 12212–12213.
27. Chu, I. K.; Rodriquez, C. F.; Lau, T. C.; Hopkinson, A. C.; Siu, K. W. M. Molecular Radical Cations of Oligopeptides. *J. Phys. Chem. B* **2000,** *104,* 3393–3397.
28. Chu, I. K.; Rodriquez, C. F.; Hopkinson, A. C.; Siu, K. W. M.; Lau, T. C. Formation of Molecular Radical Cations of Enkephalin Derivatives Via Collision-Induced Dissociation of Electrospray-Generated Copper (II) Complex Ions of Amines and Peptides. *J. Am. Soc. Mass Spectrom.* **2001,** *12,* 1114–1119.
29. Wee, S.; O'Hair, R. A. J.; McFadyen, W. D. Side-Chain Radical Losses from Radical Cations Allows Distinction of Leucine and Isoleucine Residues in the Isomeric Peptides Gly-XXX-Arg. *Rapid Commun. Mass Spectrom.* **2002,** *16,* 884–890.
30. Bagheri-Majdi, E.; Ke, Y. Y.; Orlova, G.; Chu, I. K.; Hopkinson, A. C.; Siu, K. W. M. Copper-Mediated Peptide Radical Ions in the Gas Phase. *J. Phys. Chem. B* **2004,** *108,* 11170–11181.
31. Chu, I. K.; Siu, S. O.; Lam, C. N. W.; Chan, J. C. Y.; Rodriquez, C. F. Formation of Molecular Radical Cations of Aliphatic Tripeptides from their Complexes with Cu^{II}(12-Crown-4). *Rapid Commun. Mass Spectrom.* **2004,** *18,* 1798–1802.
32. Wee, S.; O'Hair, R. A. J.; McFadyen, W. D. Comparing the Gas-Phase Fragmentation Reactions of Protonated and Radical Cations of the Tripeptides GXR. *Int. J. Mass Spectrom.* **2004,** *234,* 101–122.
33. Chu, I. K.; Lam, C. N. W.; Siu, S. O. Facile Generation of Tripeptide Radical Cations in Vacuo Via Intramolecular Electron Transfer in Cu-II Tripeptide Complexes Containing Sterically Encumbered Terpyridine Ligands. *J. Am. Soc. Mass Spectrom.* **2005,** *16,* 763–771.
34. Barlow, C. K.; McFadyen, W. D.; O'Hair, R. A. J. Formation of Cationic Peptide Radicals by Gas-Phase Redox Reactions with Trivalent Chromium, Manganese, Iron, and Cobalt Complexes. *J. Am. Chem. Soc.* **2005,** *127,* 6109–6115.
35. Lam, C. N. W.; Siu, S. O.; Orlova, G.; Chu, I. K. Macrocyclic Effect of Auxiliary Ligand on the Gas-Phase Dissociation of Ternary Copper(II)-GGX Complexes. *Rapid Commun. Mass Spectrom.* **2006,** *20,* 790–796.
36. Laskin, J.; Yang, Z.; Chu, I. K. Energetics and Dynamics of Electron Transfer and Proton Transfer in Dissociation of metal^{III}(Salen)-Peptide Complexes in the Gas Phase. *J. Am. Chem. Soc.* **2008,** *130,* 3218–3230.
37. Siu, C. K.; Ke, Y. Y.; Orlova, G.; Hopkinson, A. C.; Siu, K. W. M. Dissociation of the N–C_α Bond and Competitive Formation of the $[z_n - 23\ H]^{\bullet+}$ and $[c_n + 2H]^+$ Product Ions in Radical Peptide Ions Containing Tyrosine and Tryptophan: The Influence of Proton Affinities on Product Formation. *J. Am. Soc. Mass Spectrom.* **2008,** *19,* 1799–1807.
38. Cournoyer, J. J.; Pittman, J. L.; Ivleva, V. B.; Fallows, E.; Waskell, L.; Costello, C. E.; O'Connor, P. B. Deamidation: Differentiation of Aspartyl from Isoaspartyl Products in Peptides by Electron Capture Dissociation. *Protein Sci.* **2005,** *14,* 452–463.
39. O'Connor, P. B.; Cournoyer, J. J.; Pitteri, S. J.; Chrisman, P. A.; McLuckey, S. A. Differentiation of Aspartic and Isoaspartic Acids using Electron Transfer Dissociation. *J. Am. Soc. Mass Spectrom.* **2006,** *17,* 15–19.
40. Laskin, J.; Yang, Z. B.; Lam, C. N. W.; Chu, I. K. Charge-Remote Fragmentation of Odd-Electron Peptide Ions. *Anal. Chem.* **2007,** *79,* 6607–6614.
41. Stubbe, J.; van der Donk, W. A. Protein Radicals in Enzyme Catalysis. *Chem. Rev.* **1998,** *98,* 705–762.
42. Selmer, T.; Pierik, A. J.; Heider, J. New Glycyl Radical Enzymes Catalyzing Key. Metabolic Steps in Anaerobic Bacteria. *Biol. Chem.* **2005,** *386,* 981–988.
43. Buckel, W.; Golding, B. T. Radical Enzymes in Anaerobes. *Annu. Rev. Microbiol.* **2006,** *60,* 27–49.
44. Knappe, J.; Neugebauer, F. A.; Blaschkowski, H. P.; Ganzler, M. Post-Translational Activation Introduces a Free-Radical into Pyruvate Formate-Lyase. *Proc. Natl. Acad. Sci. U.S.A.* **1984,** *81,* 1332–1335.
45. Wagner, A. F. V.; Frey, M.; Neugebauer, F. A.; Schafer, W.; Knappe, J. The Free-Radical in Pyruvate Formate-Lyase is Located on Glycine-734. *Proc. Natl. Acad. Sci. U.S.A.* **1992,** *89,* 996–1000.
46. Mulliez, E.; Fontecave, M.; Gaillard, J.; Reichard, P. An Iron-Sulfur Center and a Free-Radical in the Active Anaerobic Ribonucleotide Reductase of*Escherichia coli. J. Biol. Chem.* **1993,** *268,* 2296–2299.
47. Coschigano, P. W.; Wehrman, T. S.; Young, L. Y. Identification and Analysis of Genes Involved in Anaerobic Toluene Metabolism by Strain T1: Putative Role of a Glycine Free Radical. *Appl. Environ. Microbiol.* **1998,** *64,* 1650–1656.
48. Leuthner, B.; Leutwein, C.; Schulz, H.; Horth, P.; Haehnel, W.; Schiltz, E.; Schagger, H.; Heider, J. Biochemical and Genetic Characterization of Benzylsuccinate Synthase from *Thauera aromatica*: A New Glycyl Radical Enzyme Catalyzing the First Step in Anaerobic Toluene Metabolism. *Mol. Microbiol.* **1998,** *28,* 615–628.
49. Selmer, T.; Andrei, P. I. P-Hydroxyphenylacetate Decarboxylase from Clostridium Difficile - A Novel Glycyl Radical Enzyme Catalyzing the Formation of p-Cresol. *Eur. J. Biochem.* **2001,** *268,* 1363–1372.
50. Raynaud, C.; Sarcabal, P.; Meynial-Salles, I.; Croux, C.; Soucaille, P. Molecular Characterization of the 1,3-Propanediol (1,3-PD) Operon of Clostridium Butyricum. *Proc. Natl. Acad. Sci. U.S.A.* **2003,** *100,* 5010–5015.
51. Eklund, H.; Fontecave, M. Glycyl Radical Enzymes: A Conservative Structural Basis for Radicals. *Structure* **1999,** *7,* R257–R262.
52. Himo, F. C–C Bond Formation and Cleavage in Radical Enzymes, a Theoretical Perspective. *Biochim. Biophys. Acta.* **2005,** *1707,* 24–33.
53. Viehe, H. G.; Janousek, Z.; Merenyi, R.; Stella, L. The Captodative Effect. *Acc. Chem. Res.* **1985,** *18,* 148–154.
54. Steill, J.; Zhao, J. F.; Siu, C. K.; Ke, Y. Y.; Verkerk, U. H.; Oomens, J.; Dunbar, R. C.; Hopkinson, A. C.; Siu, K. W. M.Structure of the Observable Histidine Radical Cation in the Gas Phase: A Captodative -Radical Ion. *Angew. Chem. Int. Ed.* **2008,** *47,* 9666–9668.
55. Tureček, F.; Carpenter, F. H. Glycine Radicals in the Gas Phase. *J. Chem. Soc. Perkin Trans.* 2. **1999,**2315–2323.
56. Tureček, F.; Carpenter, F. H.; Polce, M. J.; Wesdemiotis, C. Glycyl Radical is a Stable Species in the Gas Phase. *J. Am. Chem. Soc.* **1999,** *121,* 7955–7956.
57. Polce, M. J.; Wesdemiotis, C. First Generation and Characterization of the Enol of Glycine, H_2N-CH=$C(OH)_2$, in the Gas Phase. *J. Mass Spectrom.* **2000,** *35,* 251–257.

58. Breuker, K.; Oh, H. B.; Lin, C.; Carpenter, B. K.; McLafferty, F. W. Nonergodic and Conformational Control of the Electron Capture Dissociation of Protein Cations. *Proc. Natl. Acad. Sci. U.S.A.* **2004,** *101,* 14011–14016.
59. Pouthier, V.; Tsybin, Y. O. Amide-I Relaxation-Induced Hydrogen Bond Distortion: An Intermediate in Electron Capture Dissociation Mass Spectrometry of α-Helical Peptides? *J. Chem. Phys.* **2008,** *129,* 095106.
60. O'Connor, P. B.; Lin, C.; Cournoyer, J. J.; Pittman, J. L.; Belyayev, M.; Budnik, B. A. Long-Lived Electron Capture Dissociation Product Ions Experience Radical Migration Via Hydrogen Abstraction. *J. Am. Soc. Mass Spectrom.* **2006,** *17,* 576–585.
61. Leymarie, N.; Costello, C. E.; O'Connor, P. B. Electron Capture Dissociation Initiates a Free Radical Reaction Cascade. *J. Am. Chem. Soc.* **2003,** *125,* 8949–8958.
62. Tureček, F.; Jones, J. W.; Towle, T.; Panja, S.; Nielsen, S. B.; Hvelplund, P.; Paizs, B. Hidden Histidine Radical Rearrangements upon Electron Transfer to Gas-Phase Peptide Ions. Experimental Evidence and Theoretical Analysis. *J. Am. Chem. Soc.* **2008,** *130,* 14584–14596.
63. Hayakawa, S.; Matsubara, H.; Panja, S.; Hvelplund, P.; Nielsen, S. B.; Chen, X.; Turecek, F. Experimental Evidence for an Inverse Hydrogen Migration in Arginine Radicals. *J. Am. Chem. Soc.* **2008,** *130,* 7645–7654.
64. Weinkauf, R.; Schanen, P.; Metsala, A.; Schlag, E. W.; Burgle, M.; Kessler, H. Highly Efficient Charge Transfer in Peptide Cations in the Gas Phase: Threshold Effects and Mechanism. *J. Phys. Chem.* **1996,** *100,* 18567–18585.
65. Chu, I. K.; Zhao, J. F.; Xu, M.; Siu, S. O.; Hopkinson, A. C.; Siu, K. W. M. Are the Radical Centers in Peptide Radical Cations Mobile? The Generation, Tautomerism, and Dissociation of Isomeric α-Carbon-Centered Triglycine Radical Cations in the Gas Phase. *J. Am. Chem. Soc.* **2008,** *130,* 7862–7872.
66. Ryzhov, V.; Lam, A. K. Y.; O'Hair, R. A. J. Gas-Phase Fragmentation of Long-Lived Cysteine Radical Cations Formed Via NO Loss from Protonated S-Nitrosocysteine. *J. Am. Soc. Mass Spectrom.* **2009,** DOI: 10.1016/j.jasms.2008.12.026.
67. Rodriquez, C. F.; Cunje, A.; Shoeib, T.; Chu, I. K.; Hopkinson, A. C.; Siu, K. W. M. Proton Migration and Tautomerism in Protonated Triglycine. *J. Am. Chem. Soc.* **2001,** *123,* 3006–3012.
68. Frisch, M. J.; Trucks, G. W.; Schlegel, H. B.; Scuseria, G. E.; Robb, M. A.; Cheeseman, J. R.; Montgomery, J. A. Jr.; Vreven, T.; Kudin, K. N.; Burant, J. C.; Millam, J. M.; Iyengar, S. S.; Tomasi, J.; Barone, V.; Mennucci, B.; Cossi, M.; Scalmani, G.; Rega, N.; Petersson, G. A.; Nakatsuji, H.; Hada, M.; Ehara, M.; Toyota, K.; Fukuda, R.; Hasegawa, J.; Ishida, M.; Nakajima, T.; Honda, Y.; Kitao, O.; Nakai, H.; Klene, M.; Li, X.; Knox, J. E.; Hratchian, H. P.; Cross, J. B.; Bakken, V.; Adamo, C.; Jaramillo, J.; Gomperts, R.; Stratmann, R. E.; Yazyev, O.; Austin, A. J.; Cammi, R.; Pomelli, C.; Ochterski, J. W.; Ayala, P. Y.; Morokuma, K.; Voth, G. A.; Salvador, P.; Dannenberg, J. J.; Zakrzewski, V. G.; Dapprich, S.; Daniels, A. D.; Strain, M. C.; Farkas, O.; Malick, D. K.; Rabuck, A. D.; Raghavachari, K.; Foresman, J. B.; Ortiz, J. V.; Cui, Q.; Baboul, A. G.; Clifford, S.; Cioslowski, J.; Stefanov, B. B.; Liu, G.; Liashenko, A.; Piskorz, P.; Komaromi, I.; Martin, R. L.; Fox, D. J.; Keith, T.; Al-Laham, M. A.; Peng, C. Y.; Nanayakkara, A.; Challacombe, M.; Gill, P. M. W.; Johnson, B.; Chen, W.; Wong, M. W.; Gonzalez, C.; Pople, J. A. *Gaussian 03, Revision D. 01*; Gaussian Inc.: Wallingford, CT, 2004.
69. Becke, A. D. Density-Functional Thermochemistry. 3. The Role of Exact Exchange. *J. Chem. Phys.* **1993,** *98,* 5648–5652.
70. Lee, C. T.; Yang, W. T.; Parr, R. G. Development of the Colle-Salvetti Correlation-Energy Formula into a Functional of the Electron-Density. *Phys. Rev. B* **1988,** *37,* 785–789.
71. Hehre, W. J.; Ditchfie, R.; Pople, J. A. Self-Consistent Molecular-Orbital Methods. 12. Further Extensions of Gaussian-Type Basis Sets for Use in Molecular-Orbital Studies of Organic-Molecules. *J. Chem. Phys.* **1972,** *56,* 2257–2261.
72. Clark, T.; Chandrasekhar, J.; Spitznagel, G. W.; Schleyer, P. V. Efficient Diffuse Function-Augmented Basis-Sets for Anion Calculations. 3. The 3-21+g Basis Set for First-Row Elements, Li-F. *J. Comput. Chem.* **1983,** *4,* 294–301.
73. Merrick, J. P.; Moran, D.; Radom, L. An Evaluation of Harmonic Vibrational Frequency Scale Factors. *J. Phys. Chem. A* **2007,** *111,* 11683–11700.
74. Reed, A. E.; Weinstock, R. B.; Weinhold, F. Natural-Population Analysis. *J. Chem. Phys.* **1985,** *83,* 735–746.
75. Baer, T.; Hase, W. L. *Unimolecular Reaction Dynamics: Theory and Experiments;* Oxford: New York, 1996; p. 188–210.
76. Baer, T.; Mayer, P. M. Statistical Rice-Ramsperger-Kassel-Marcus Quasiequilibrium Theory Calculations in Mass Spectrometry. *J. Am. Soc. Mass Spectrom.* **1997,** *8,* 103–115.
77. Beyer, T.; Swinehart, D. F. Number of Multiply-Restricted Partitions. *Commun. ACM* **1973,** *16,* 379–379.